NUMERICAL SIMULATIONS OF THERMAL ENERGY STORAGE SYSTEMS WITH PHASE CHANGE MATERIALS

P. A. Galione[1,3], O. Lehmkuhl[1,2], J. Rigola[1], A. Oliva[1], I. Rodríguez[1]

[1] Centre Tecnològic de Transferència de Calor (CTTC), Universitat Politècnica de Catalunya (UPC), ETSEIAT, C. Colom 11, 08222 Terrassa, Barcelona (Spain). Fax: +34 93 739 89 20, e-mail: cttc@cttc.upc.edu

[2] Termo Fluids S.L., Magi Colet 8, 08204 Sabadell, Barcelona (Spain). E-mail: termofluids@termofluids.com

[3] Instituto de Ingeniería Mecánica y Producción Industrial, Universidad de la República (Uruguay)

1. Introduction

Thermal energy storage systems are an essential feature to make an efficient use of solar energy due to the inherent intermittence of this energy source. These systems allow making use of thermal energy - accumulated in hours of high solar radiation - in moments of lower solar radiation, reducing the mismatch between the supply and demand of the energy. Phase change materials (PCM) provide an effective way of accumulating thermal energy, due to their high capacity to store heat at a constant or near to constant temperature.

This paper deals with the numerical simulation of thermal energy storage systems with PCM. Numerical simulations are a powerful tool for predicting the thermal behaviour of thermal systems, as well as for optimizing their design.

The system under study is a cylindrical container, filled with spheres containing paraffin wax (PCM) and water occupying the space left between the spheres. Two different processes are studied: charging and discharging. In charging mode, hot water coming from the solar field passes through the container, delivering energy to the PCM spheres. In the discharging mode, cold water from supply comes through, extracting the energy previously stored in the PCM and leaving the tank at a higher temperature.

Firstly, a simplified study similar to the presented by Felix Regin et al. (2009) and Bédérrecats et al. (2009) is developed, where assumptions of one dimensional fluid flow and one dimensional heat transfer - in the flow and inside the spheres – are made. Results of liquid fraction, outlet temperature and accumulated energy are presented. Comparison against previous works is carried out.

Secondly, in order to account for natural convection inside the PCM spheres, detailed CFD simulations of the solid-liquid phase change are performed using the fixed-grid enthalpy-porosity model (Brent et al., 1988; Voller and Prakash, 1987). Verification and validation of the phase change modelling are performed against previous numerical and experimental results (Costa et al., 1991; Gau and Viskanta, 1986). The CFD code is used for modelling the PCM inside the spheres and it is coupled with the simple 1D model of the water, resulting in a more detailed model of the entire system. Simulations of the charging and discharging modes are performed and results obtained are compared against previous 1D analysis results.

2. Mathematical formulation and numerical issues

In this section, the mathematical formulation is presented for simple 1D and detailed 2D analyses and the numerical aspects detailed.

2.1. Simplified modelling (1D)

The mathematical formulation for the heat exchanging fluid (water in the cases studied here) is based on both mass and energy conservation equations. Simplifying assumptions are:

- One-dimensional fluid flow and temperature distribution (in the flow direction).
- Constant density and specific heat.
- Heat conduction in flow direction is not considered.
- Ambient losses are negligible.
- Negligible radiation transfer.

Nomenclature

A surface area of the cylindrical container, m^2	S momentum source term coefficient, kg m^{-3} s^{-1}
A_{sph} external surface area of PCM spheres, m^2	Ste Stefan number
A_r aspect ratio, A_r = *height/width*	T temperature, ºC
C_p specific heat, J kg^{-1} K^{-1}	t time, s
D diameter, m	**u** velocity vector, m s^{-1}
Fo Fourier number	V volume, m^3
h convective heat transfer coefficient, W m^{-2} K^{-1}	β volumetric thermal expansivity, K^{-1}
H enthalpy, J	μ dynamic viscosity, N s m^{-2}
k thermal conductivity, W m^{-1} K^{-1}	ρ density, kg m^{-3}
L latent heat of fusion, J kg^{-1}	τ dimensionless time, $\tau = Fo\ Ste\ A_r^2$
$\dot{m}$ mass flow rate, kg s^{-1}	
p pressure, N m^{-2}	*Subscripts and Superscripts*
r radius, m	f fluid
R resistance to heat transfer, K W^{-1}	l liquid PCM
Ra Rayleigh number	s solid PCM
Re Reynolds number	cap_ext outer surface of a capsule
Pr Prandtl number	cap_int inner surface of a capsule

For the PCM spheres the mathematical formulation is based on energy conservation property, with the following assumptions:

- One-dimensional heat transfer.
- Only conduction is considered as the heat transfer phenomena.
- Constant density.
- Constant solid and liquid specific heats, but different between them.
- Negligible conduction between different spheres.
- Negligible radiation transfer.

The equations are discretized using the Finite Volume Method as detailed below.

The cylindrical container is divided in N_x equal parts in the axial direction, in which fluid temperature is considered uniform (see Figs. 1 and 2). The spheres are discretized in N_r parts along the radial direction (Fig.2). As 1D conditions are assumed, all the spheres in the same section of container have the same temperature distributions; therefore, only one sphere per section is simulated.

Fluid temperature equations:

$$\rho V_i C_p \frac{\partial T_i}{\partial t} = -\dot{m} C_p \left(T_i^{out} - T_i^{in}\right) - h_i A_{sph,i} \left(T_i - T_i^{cap\_ext}\right); \text{ where } h = \frac{k.Nu}{D_{cap\_ext}} \qquad \text{(Eq. 1)}$$

$$Nu = 2.0 + 1.1 \mathrm{Re}^{0.6} \mathrm{Pr}^{1/3}, \quad 15 < \mathrm{Re} < 8500; \text{ (Wakao et al., 1979)} \qquad \text{(Eq. 2)}$$

$$Nu = 18.1 \mathrm{Pr}^{1/3}, \quad \mathrm{Re} < 40; \text{ (Vafai and Sozen, 1990)} \qquad \text{(Eq. 3)}$$

Where sub index i indicates the tank section where the temperature is being calculated, T^{out} and T^{in} are the temperatures of outgoing and ingoing flows from and into the control volume and T^{cap_ext} the temperature of the PCM capsule external surface. Here, Reynolds number is calculated using the superficial

velocity: $\mathrm{Re} = \frac{\dot{m}}{A}\frac{D_{cap\_ext}}{\mu}$. As the ranges of validity of Eqs. 2 and 3 are intersected, two different values of *Nu* are obtained for the same *Re*; then, the highest of both was considered.

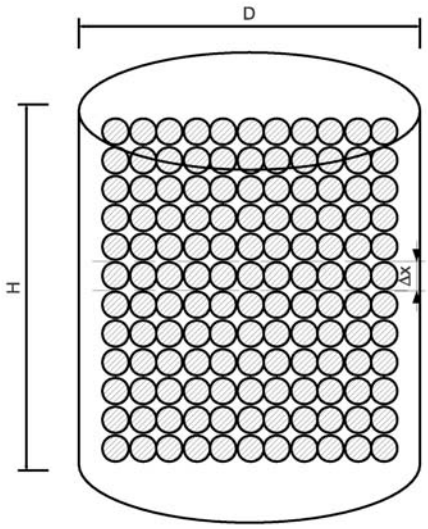

Fig. 1: Sketch representing the cylindrical container with the encapsulated PCM.

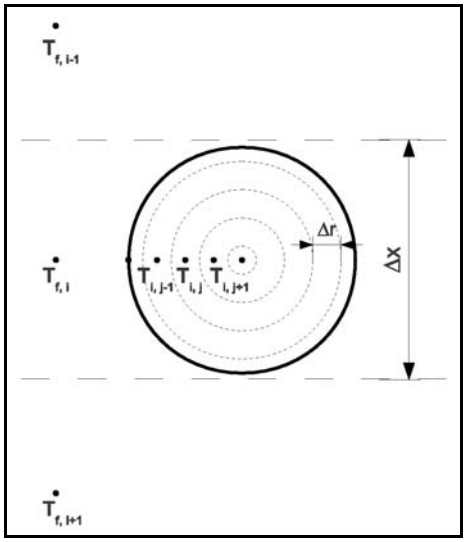

Fig. 2: Discretization details of the tank and of a representative sphere.

Sphere temperature equations, inner nodes:

$$\frac{\partial H_{i,j}}{\partial t} = \left(kA\frac{\partial T}{\partial r}\right)_{i,j-1/2} - \left(kA\frac{\partial T}{\partial r}\right)_{i,j+1/2} \qquad \text{(Eq. 4)}$$

Where the sub indices *j-1/2* and *j+1/2* indicate the boundaries of the control volume *j*, near to the wall and to the center of the sphere, respectively.

Sphere temperature equations, boundary node:

$$\frac{\partial H_{i,j}}{\partial t} = \frac{T_{f,i} - T_{i,0}}{R_{conv} + R_{cap}} - \left(kA\frac{\partial T}{\partial r}\right)_{i,1/2} \qquad \text{(Eq. 5)}$$

Where $R_{conv} = \frac{1}{h_{f,i} A_{cap\_ext}}$ and $R_{cond} = \frac{1}{4\pi k_{shell}\left(\frac{1}{r_{cap\_int}} - \frac{1}{r_{cap\_ext}}\right)}$

To solve these equations, it is necessary to define a relation between enthalpy and temperature of the PCM. The material used as PCM in this work is paraffin wax, which has a range of phase change temperatures rather than a unique temperature (i.e. during heating there is an increase in temperature between the onset and the end of the melting process). Therefore, a function that relates enthalpy and temperature can be defined. Nevertheless, as a first approximation we are also interested in modelling the constant temperature phase change, because in the CFD simulations described in the next subsection this condition is assumed.

The enthalpy – temperature relation is defined by eqs. 6 - 8 for the constant temperature phase change and by eqs. 13 - 16 for the variable phase change temperature, similarly as Felix Regin et al. (2009).

Constant phase change temperature:

$$\frac{H}{\rho V} = C_{ps} T, \quad T < T_{sl} \qquad \text{(Eq. 6)}$$

$$\frac{H}{\rho V} = C_{ps} T + f.L \text{ with } f = \frac{H - H_s}{L}; \quad H_s < H < H_l, \quad T = T_{sl} \qquad \text{(Eq. 7)}$$

$$\frac{H}{\rho V} = C_{pl}\left(T - T_{\mathrm{sl}}\right) + C_{ps}T_{\mathrm{sl}} + L, \quad T > T_{sl} \qquad \text{(Eq. 8)}$$

Here T_{sl} indicates the phase change temperature.

Variable phase change temperature:

$$\frac{H}{\rho V} = C_{ps}T, \quad T \le T_s \qquad \text{(Eq. 9)}$$

$$\frac{H}{\rho V} = C_{ps}T + \frac{L}{T_l - Ts}\left(T - T_s\right), \quad T_s < T \le T_{\mathrm{sl}} \qquad \text{(Eq. 10)}$$

$$\frac{H}{\rho V} = C_{pl}\left(T - T_{\mathrm{sl}}\right) + C_{ps}T_{\mathrm{sl}} + \frac{L}{T_l - Ts}\left(T - T_s\right), \quad T_{\mathrm{sl}} < T < T_l \qquad \text{(Eq. 11)}$$

$$\frac{H}{\rho V} = C_{pl}\left(T - T_{\mathrm{sl}}\right) + C_{ps}T_{\mathrm{sl}} + L, \quad T \ge T_l \qquad \text{(Eq. 12)}$$

Where T_{sl} indicates the temperature in the phase change range ($T_s < T_{sl} < T_l$) beyond which the material has a mostly liquid behavior, and below which it behaves mostly as solid.

Actually, in the 1D model, variable phase change formulation is used to simulate constant phase change by defining T_s and T_l very close to T_{sl}. This strategy is adopted because 1D analysis was based on finding temperature values instead of enthalpy values, so there is a need to be able to identify every state with its temperature, which is not verified by the constant phase change formulation. However, for the detailed CFD analysis, the above indicated formulation is indeed used.

For the temporal discretization a fully implicit scheme is chosen. Furthermore, an upwind-like scheme is used to determine the temperatures of the flow entering and leaving each section. Thus, the temperature of the fluid entering each section of the tank becomes the same as the temperature of the fluid in the upstream section, and the leaving fluid temperature the same as the one of the present section. This scheme allows to adopt a step by step method to solve the entire tank, first solving the section where the inlet is placed (in the top or bottom of the tank), then the next section downstream, and so on advancing in the direction of the flow, without needing to iterate.

In each section, fluid and PCM temperatures have to be solved. The final matrix of coefficients derived from the system of equations in each container section has a tri-diagonal pattern, thus a TDMA algorithm is used to solve the linear system. This formulation is implemented in a simple computer code intended to simulate the behavior in charging and discharging modes of the whole energy accumulation system. A simulation of 10 hours of operation takes only a few seconds of computations in a single conventional CPU core (here used: Intel Core i-5 2300 2.8GHz).

Current formulation includes the implicit assumption that there is no need to refine the container subdivisions further than one sphere's diameter high; as it is considered that each sphere "sees" a uniform temperature of fluid. This constraint does not allow modelling a system with "big" spheres that make this assumption too coarse. However, as our intention was to simulate an efficient energy accumulation device, it is acceptable to think that the size of sphere used would be much smaller than the height of the tank, in order to maximize the relation of heat transfer area over volume of PCM.

Results presented in this work were obtained wit N_x = 24 and N_r = 12. Some tests have been carried out with finer grids, and the results obtained were very close to the presented here, indicating acceptable grid independence.

2.2. Detailed modelling of the phase change (2D - 3D)

When the PCM inside the spheres are changing phase, natural convection is produced due to the difference between solid and liquid densities and gravity action. To simulate this phenomenon, Navier-Stokes and energy equations are numerically solved. Some simplyfying assumptions are made:

- Incompressible fluid.

- Boussinesq aproximation (density is considered constant, except in the gravity forces term).
- Constant thermo-physical properties (properties of solid and liquid states are assumed to be equal).

Based on the above mentioned hypotheses and considering the enthalpy model to account for the phase change phenomenon (Voller and Prakash, 1987; Brent et al., 1988), mass, momentum and energy equations can be written in the following form:

$$\nabla.\mathbf{u} = 0 \qquad \text{(Eq. 13)}$$

$$\frac{\partial \rho \mathbf{u}}{\partial t} + \mathbf{u}.\nabla(\rho \mathbf{u}) = -\nabla p + \mu \nabla^2 \mathbf{u} + \rho \mathbf{g} + S.\mathbf{u} \qquad \text{(Eq. 14)}$$

$$\frac{\partial H}{\partial t} + \nabla.(\rho \mathbf{u} C_{pl} T) = \nabla.(k \nabla T) \qquad \text{(Eq. 15)}$$

The source term $S.\mathbf{u}$ is introduced into the momentum equation to account for the presence of solid in the control volumes. Its final form depends on the porosity (or liquid fraction), as explained in Voller and Prakash (1987) and in Brent et al. (1988).

These equations are discretized using an explicit Finite Volume Method. The velocity-pressure coupling is resolved by adopting a Fractional Step Method. The adoption of the enthalpy method allows working with a fixed grid instead of an interface tracking method.

As in this approach an explicit time scheme is used, the momentum source term intended to model the presence of solid is only needed in the control volumes that contain solid and liquid, not in the pure solid containing volumes, as in these a zero velocity can be imposed explicitly.

The final form of the source term coefficient (S) depends on the approximation adopted for the behavior of the flow in the "mushy zone" (where mixed solid and liquid states are present). However, in the case of constant phase change temperature, the solid-liquid interface should be of infinitesimal width (although it cannot be thinner than one control volume width in our simulations); therefore, the formulation used for the source term is not very important in a physical sense, as long as it manages to bring the velocity to zero in mostly solid control volumes and to vanish if the volume contains pure liquid.

The solid-liquid formulation was implemented into a previously developed CFD code (Lehmkuhl et al., 2009) intended to work with unstructured meshes and parallel computing.

To simulate the entire system (container with water and PCM spheres), the detailed CFD code was used to simulate the spheres assuming 2D behavior and coupled with the simple water flow 1D model previously described.

The tank was subdivided in 24 sections (N_x = 24). As in the simple 1D model, only one sphere is simulated in each division, assuming that all the spheres in a section have the same behaviour.

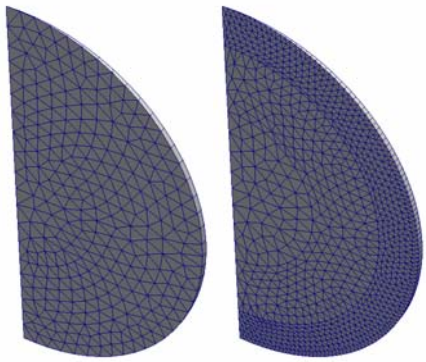

Fig. 3: meshes of PCM spheres. Left: actual mesh used for simulations. Right: mesh used to test accuracy of the results obtained with the previous mesh.

Each sphere was simulated using a 2D mesh of a slice, divided in 547 control volumes (see Fig. 3, left). Some tests were made to check the mesh density suitability, simulating one sphere with a mesh of 1774 control volumes (Fig. 3, right) and having the same boundary conditions as the sphere of the first tank subdivision. The obtained results, although not exactly equivalent, were sufficiently close (normally less than 5% of discrepancy in local liquid fraction and less than 1% in local fluid temperature).

This more detailed model of the system is much more costly in terms of computational requirements than the previous 1D model. Both cases of study (charging and discharging) were run on 48 CPU cores running in

parallel (AMD Opteron Barcelona 2.1 GHz, Infiniband network 4X-DDR 20Gb/s). Charging mode was more demanding than discharging, taking around 4 days of computations to simulate 5 hours of operation.

3. Verification and Validation of the detailed phase change modelling

The CFD model described in previous section was verified and validated using experimental and numerical results found in the bibliography.

3.1 Gallium melting

Firstly, a case of Gallium melting in a rectangular cavity (Gau and Viskanta, 1986; Costa et. al., 1991; Vidal, 2007) was simulated. The problem is 2D and consists of a rectangular cavity of aspect ratio A_r = 0.5 filled with Gallium in solid state. Top and bottom walls are adiabatic, while left and right walls are set to uniform temperatures. Initially, all the system is at a temperature slightly below phase change. Suddenly, the left wall temperature is increased above phase change and heat starts to enter the cavity, melting the Gallium. Natural convection is observed and the phase change interface starts to be deformed from its initial vertical-line shape.

The parameters of the problem are the following:

- Aspect ratio, A_r = 0.5, H (*height)* = 0.0445 m;
- ρ = 6093 kg m^{-3}, k = 32 W m^{-1} K^{-1}, C_p = 381.5 J kg^{-1} K^{-1};
- *Ra* = 2.1E5, *Pr* = 0.0216, *Ste* = 0.0419.
- Initial temperature of 28.3ºC, hot wall temperature of 38ºC and phase change temperature of 29.78ºC.

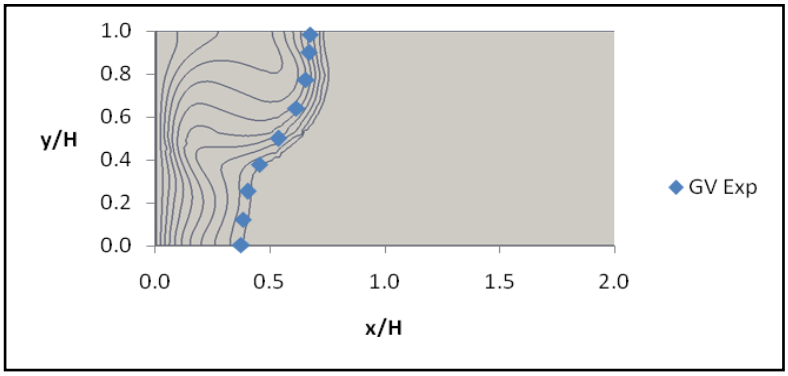

Fig. 4: Temperature contours and solid-liquid interface position of the melting Gallium in the rectangular cavity, at time t = 6 min. The dots indicate the location of the interface obtained experimentally by Gau and Viskanta (1986).

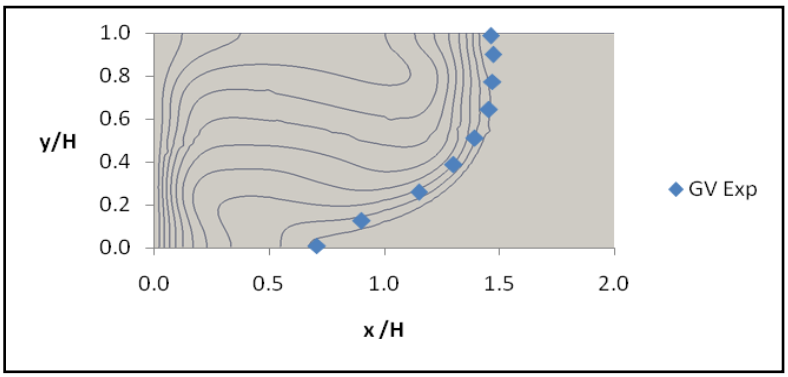

Fig. 5: Temperature contours and solid-liquid interface position of the melting Gallium in the rectangular cavity, at time t = 17 min. The dots indicate the location of the interface obtained experimentally by Gau and Viskanta (1986).

Figures 4 and 5 show the interface position as well as temperature contours and fig. 6 shows a correlation between $Nu/Ra^{-0.25}$ and non-dimensional time τ as in Gau and Viskanta (1986) . Results obtained are very similar to previous numerical ones from Costa et al. (1991) and very close to experimental ones, as it is shown in the above figures. Some causes of discrepancy between numerical and experimental results might

be found in the facts that in the experimental setup the configuration is not exactly 2D (presence of front and back walls) and that left wall temperature does not reach its final value until some time has passed.

Different mesh densities have been used, and results show that a mesh density of 80 x 40 is enough to obtain accurate results.

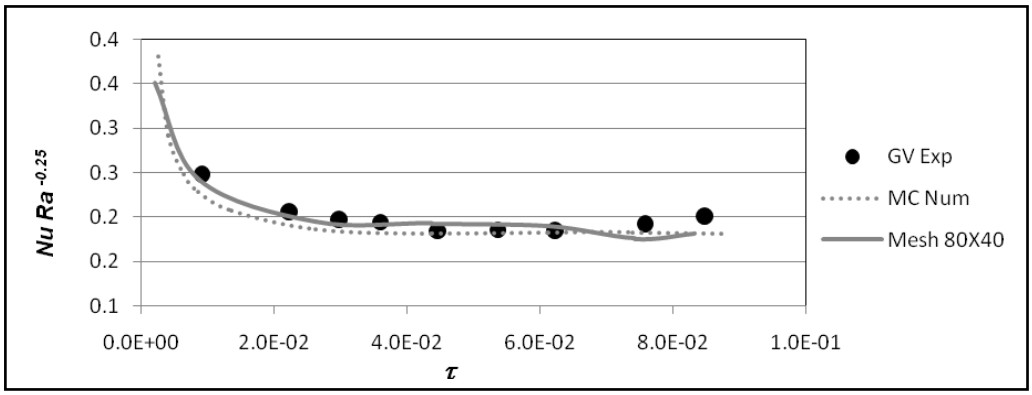

Fig. 6: Evolution of Nu $Ra^{-0.25}$ with non-dimensional time τ = Fo*Ste*A_r^2 (as in Gau and Viskanta, 1986). GV Exp: experimental results from Gau and Viskanta (1986). MC Num: Numerical results from Costa et al. (1991).

3.2 Spheres filled with N-octadecane

Another case study used to validate the CFD phase change model is the melting of a sphere of N-octadecane, as in Tan (2008) and Tan et al. (2009). A spherical capsule is filled with this material and taken to a temperature 1ºC below the phase change. Suddenly the spherical capsule shell is heated and maintained at a constant temperature. Again, the phenomenon is assumed to be 2D. Parameters of the problem are:

- D (diameter of sphere) = 0.10166 m;
- ρ = 772 kg m^{-3}, k = 0.1505 W m^{-1} K^{-1}, C_p = 2330 J kg^{-1} K^{-1};
- Ra = 3.307E7, Pr = 59.76, Ste = 0.112913.
- Initial temperature of 27.2ºC, hot wall temperature of 40ºC and phase change temperature of 28.2ºC.

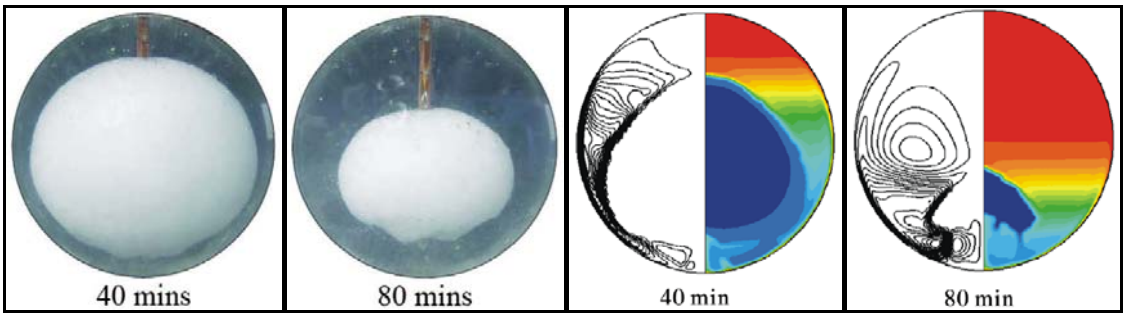

Fig. 7: Fist two are photographs of the experiment run by Tan (2008) with N-Octadecane encapsulated in a sphere, at 40 and 80 minutes of operation. The last are simulations results obtained by Tan et. al. (2009), intended to reproduce their previous experimental results. First half of the simulated spheres show streamlines while second half show temperature contours.

Fig.7 shows two photographs of the experimental evolution of the phase change at different moments extracted from Tan (2008) and some results of the simulations performed by Tan et al. (2009). Fig. 8 shows some graphical results obtained by the present work. The mesh used in our simulations was designed to have similar quantity of nodes – between 7600 and 7700 cells - as the one used by Tan et al. (2009). There is an agreement in the overall behavior of the system, although a faster melting is encountered in numerical results from both authors, compared to experimental. However, it can be seen that the results presented on our work seem to be closer to experimental than the presented by Tan et al. (2009).

As in the Gallium melting case, the faster melting obtained by the numerical simulations might be explained by the fact that a sudden increase in the capsule shell temperature is assumed, while in the experimental setup there is a natural delay in this temperature increase.

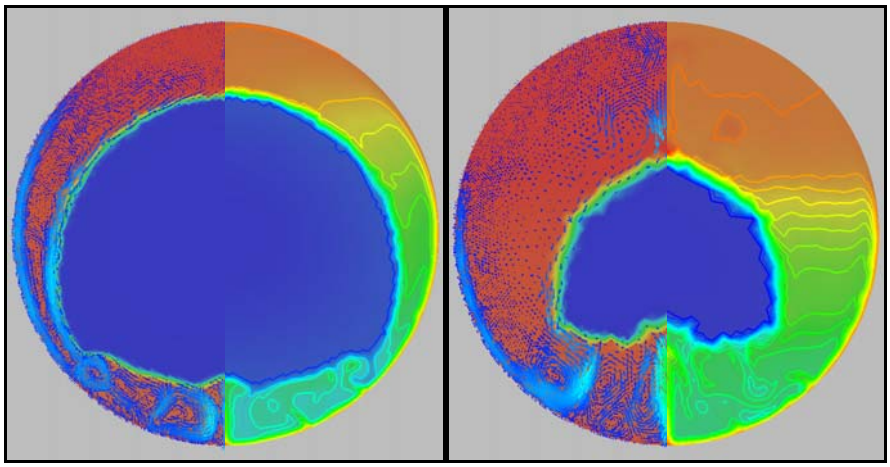

Fig. 8: Results of present work simulations at 40 min (left) and at 80 min (right). The left half of the spheres shows the enthalpy map (colour) and the velocity vectors, while the right half shows the temperature map (colour) and contours.

4. Results and discussion

In this section, the results of simulating the charging and discharging modes of operation of the thermal energy accumulation system are presented. Following parameters were used in both modes:

- Container dimensions: H (height) = 1.5 m, D (diameter) = 1.0 m
- Capsules dimensions: ϕ_{ext} (outer diameter) = 0.04 m, w (capsule thickness) = 0.0004 m
- Paraffin wax as PCM. Thermo-physical properties used are listed in Table 1.
- Capsules material: stainless steel.
- Water flow, $\dot{m}$ = 0.0796 kg/s.

Tab. 1: Thermo-physical properties of paraffin wax used as PCM.

ρ (kg/m^3)	C_{ps} (J/kg K)	C_{pl} (J/kg K)	k_s (W/m K)	k_l (W/m K)	L (kJ/kg)	β (K^{-1})	μ (N s/m)	T_{sl} (ºC)	T_s (ºC)	T_l (ºC)
850	2000	2150	0.24	0.22	190	9.1E-4	4.42E-3	59.9	52.9	61.6

4.1 Charging mode

In charging mode, the whole system is initially at a uniform temperature of 50ºC, and a water flow at 70ºC starts entering the tank through the top. Spheres, which were initially at solid state, start to receive heat and eventually to melt.

Fig. 9 shows a detail of the liquid flow, enthalpy and temperature maps of a representative sphere in the first section of tank in charging mode, simulated with the CFD model, with the finest mesh considered (Fig. 3, right). Natural convection phenomenon is clearly identified.

An ascending flow is induced by the higher temperature of the fluid at the capsule shell, arriving to the top of the sphere and then descending to come into contact with the solid part. The liquid fow transfers some of its heat to the solid, getting cooler and descending along the solid boundary.

As the temperature of the capsule is higher than the inner temperature also at the bottom of the sphere, another ascending flow is generated here, with an opposite spinning sense to the one of the main flow. This flow produces a high heat transfer rate locally, accelerating the melting process at the bottom and deforming the initially spherical shape of the solid portion.

The resulting temperature map and solid shape are appreciably different from the concentric ones that would be obtained if the convection were not present.

It should be noted that, in this work, forces acting on the solid have not been considered. These tend to bring the solid portion down to the bottom of the capsule at some moment of the melting, as shown by Tan (2008), deviating its evolution from the described by our model. These effects should be considered in future works.

The numerical results of the simulations of the whole system (tank + capsules) are shown in Figs.10 - 14, where simplified analysis for constant and variable phase change temperature, as well as detailed constant phase change temperature are included.

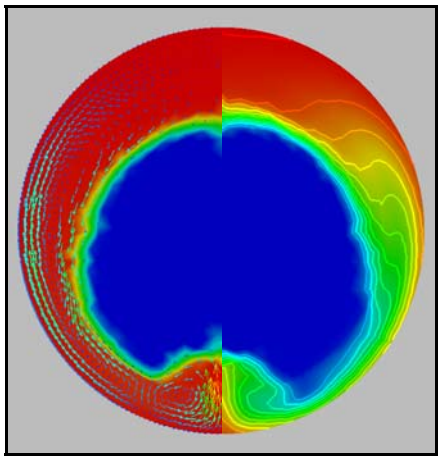

Fig. 9: Detail of the first sphere in the tank, in charging mode. Left half shows the enthalpy map and velocity vectors, while right half shows the temperature map and contours.

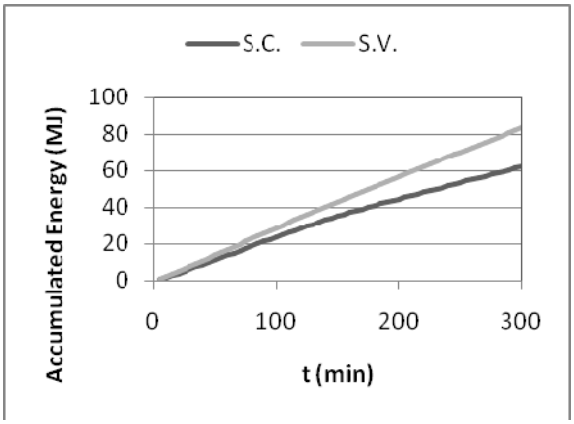

Fig. 10: Evolution of the global accumulated energy in the PCM spheres. Charging mode. S.C.: Simple, constant phase change model. S.V. : Simple, variable ph. ch. model.

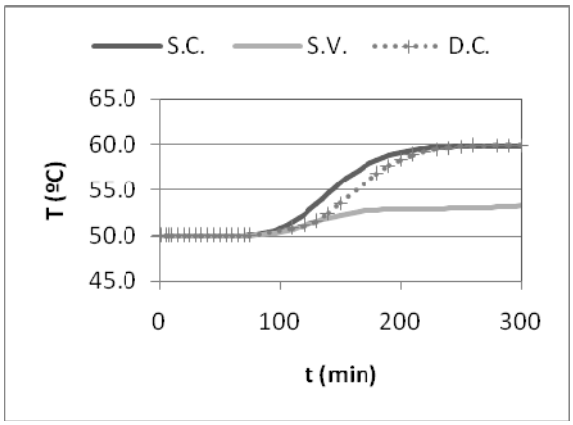

Fig. 11: Outlet fluid temperature vs. time. Charging mode. S.C.: Simple, constant phase change model. S.V. : Simple, variable ph. ch. model. D.C.: Detailed const. ph. ch. model.

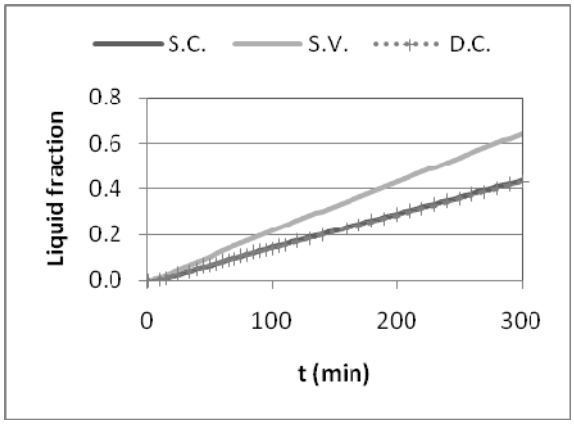

Fig. 12: Global liquid fraction. Charging mode. S.C.: Simple, constant phase change model. S.V. : Simple, variable ph. ch. model. D.C.: Detailed const. ph. ch. model.

Comparing simplified and detailed model for the constant phase change temperature case, it is observed that the differences are rather marginal, especially in the evolution of the global liquid fraction (Fig. 12), where almost no differences are encountered. However, looking at the evolution of the outlet fluid temperature (Fig. 11) and at the local liquid fraction over time (Figs. 13 and 14), some discrepancies are revealed, although not very pronounced. From these observations it is concluded that for this case of study the convection is not a very important phenomenon in a global sense, although its effects of enhancing the heat transfer are noticeable at some scale.

However, when comparison is made between constant and variable phase change, quite pronounced differences are observed. Figs. 10-12 reveal that the effectiveness of the heat accumulation system is enhanced appreciably by the variable phase change temperature. Phase change starts before than in the constant temperature case (at 52.9ºC instead of 59.9ºC) causing an earlier increase in the heat transfer rate (see Figs. 13-14), and thus a faster lowering of the water temperature. This is due to the higher thermal inertia of the mixed solid-liquid phase state than that of the pure solid phase. These observations are in concordance with Felix Regin et al. (2009); although results are not the same, which is probably due to the

differences in the assumptions adopted in both analyses.

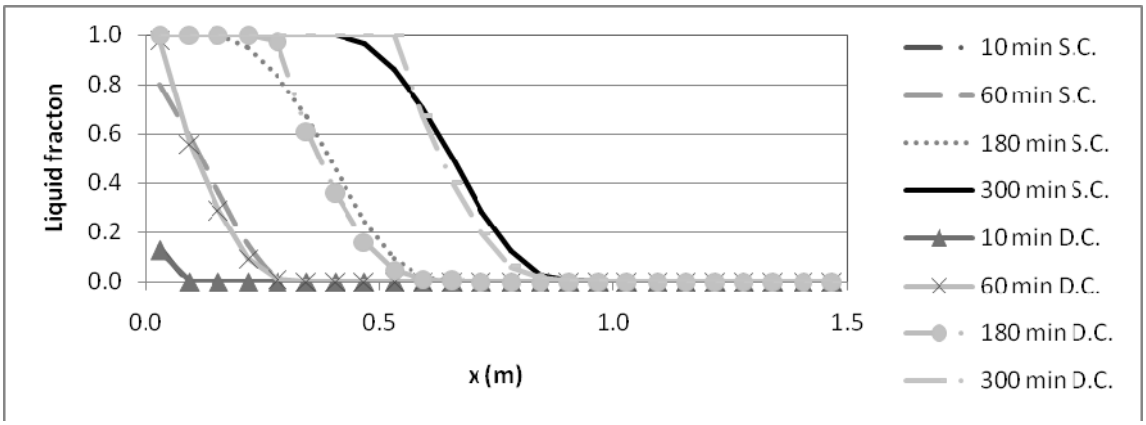

Fig. 13: Local liquid fraction vs. position in the container, at several moments. Charging mode. S.C.: Simple, constant phase change model. D.C.: Detailed const. ph. ch. model.

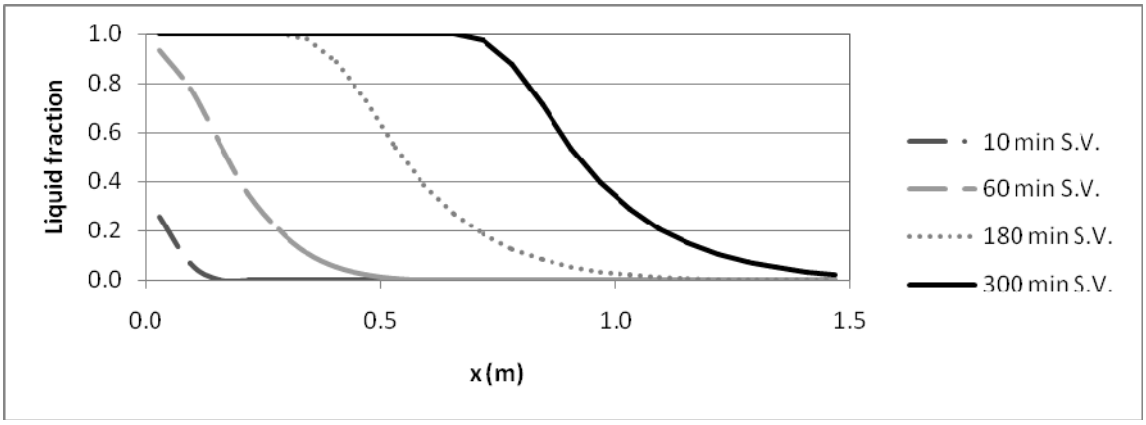

Fig. 14: Local liquid fraction vs. position in the container, at several moments. Charging mode. S.V. : Simple, variable phase change model.

4.2. Discharging mode

Discharging mode is characterized by an initial state of uniform temperature of 70ºC of the whole system, and a water flow entering at 50ºC from the bottom of the container. The PCM, initially in the liquid state, starts to release heat though the capsule shell and eventually to solidify.

In this case, the detailed simulations show that although natural convection is indeed produced, it does not have a strong effect on interface shapes nor on temperature distributions, which are almost exactly concentric to the spherical capsule shell.

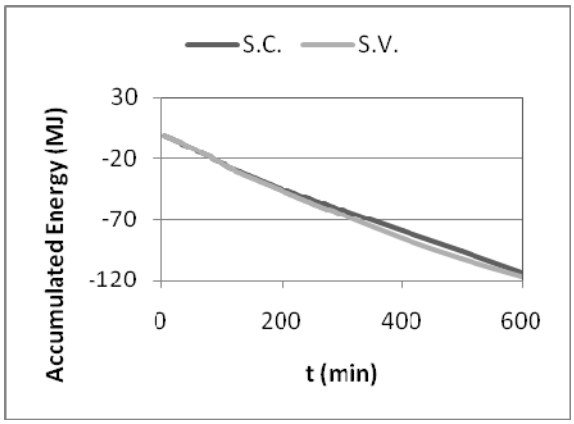

Fig. 15: Evolution of the global accumulated energy in the PCM capsules. Discharging mode. S.C.: Simple, constant phase change model. S.V. : Simple, variable ph. ch. model.

Figs. 15-19 show the numerical results obtained by the different simulations. It is observed that in this case there are almost no deviations between results from different models. This is most likely due to the fact that solidification starting temperature is very similar between constant temperature (59.9ºC) and variable temperature phase change (61.6ºC) cases, making almost negligible the difference in solidification onset moments and thus in heat transfer rates. Results obtained with the detailed model are even closer to the simple 1D analysis than in charging mode. This agrees with the previous observations regarding detailed simulations.

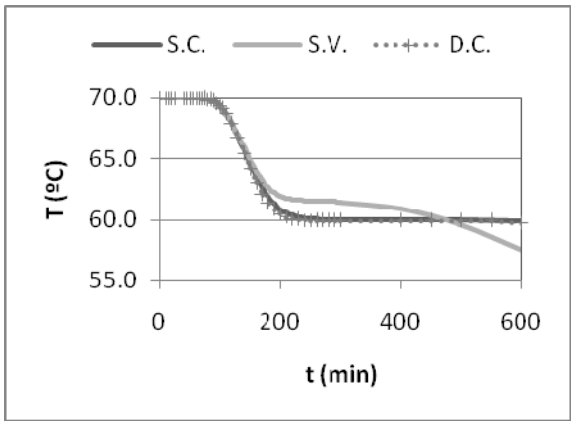

Fig. 16: Outlet fluid temperature vs. time. Discharging mode. S.C.: Simple, constant phase change model. S.V. : Simple, variable ph. ch. model. D.C.: Detailed const. ph. ch. model.

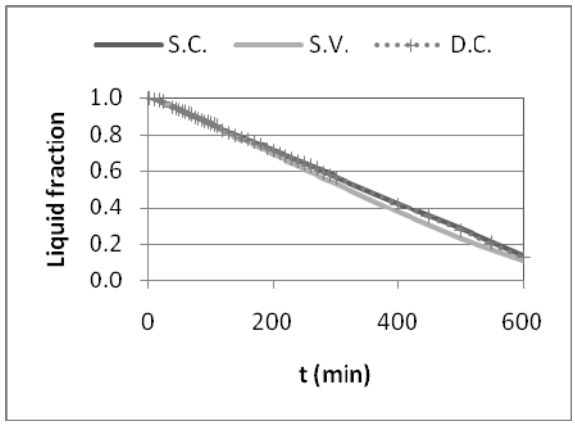

Fig. 17: Global liquid fraction. Discharging mode. S.C.: Simple, constant phase change model. S.V. : Simple, variable ph. ch. model. D.C.: Detailed const. ph. ch. model.

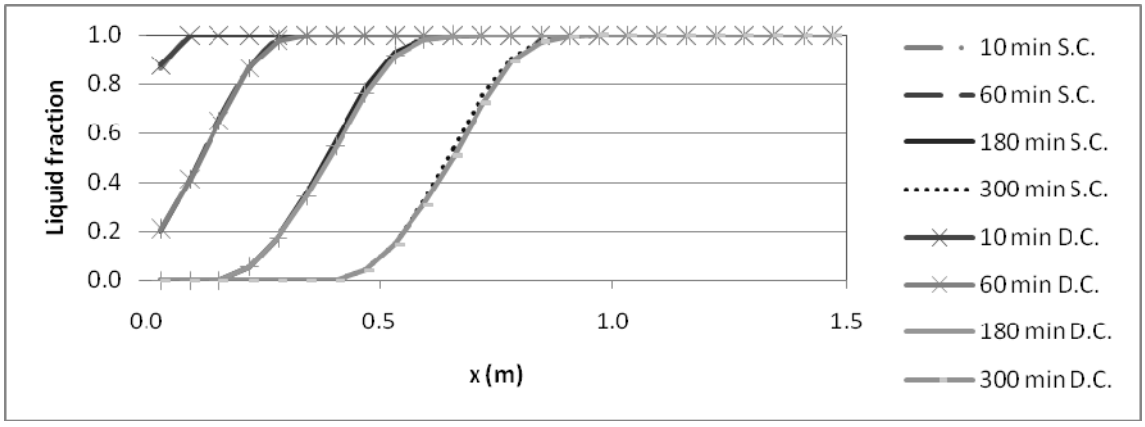

Fig. 18: Local liquid fraction vs. position in the container, at several moments. Discharging mode. S.C.: Simple, constant phase change model. D.C.: Detailed const. ph. ch. model.

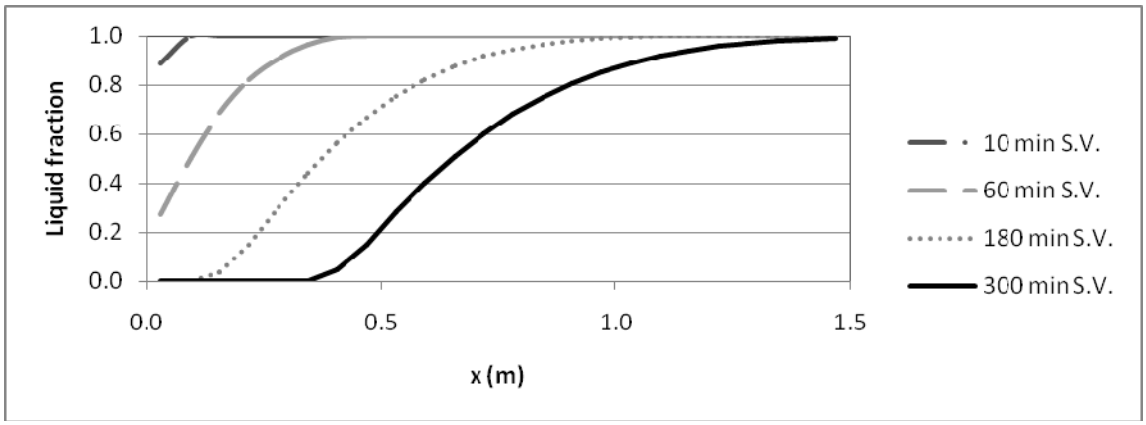

Fig. 19: Local liquid fraction vs. position in the container, at several moments. Discharging mode. S.V. : Simple, variable phase change model.

5. Conclusions

Simple 1D analysis, as well as a more detailed one including CFD calculations for the PCM have been performed in order to simulate the performance of a thermal energy accumulation system.

Fixed grid enthalpy-porosity model of the solid-liquid phase change has been succesfully implemented in a parallel unstructured CFD code. Simulations were verificated and validated against numerical and experimental data found in the bibliography.

Natural convection produced in the melting of the PCM inside spherical capsules has been observed to have noticeable effects on the solid-liquid interface shape and on the temperatures distribution. However, for the cases studied in this paper, simple-1D and detailed models considering a constant phase change temperature

give very similar results for the whole system. This would indicate that natural convection is not a determinant phenomenon of the global behaviour of this system in these cases. However, it should be noted that convection could have significant effects under other operation conditions.

On the other hand, remarkable differences in the global system performance have been observed indeed between the simulations considering constant and variable phase change temperature. Better results were obtained in the variable phase change temperature case. Future work should be carried out in performing CFD calculations taking into account this physical characteristic of the PCM.

Future work should also consider the mobility of the solid parts.

6. References

Bédérrecats, J.P., Castaing-Lasvignottes, J., Strub, F., Dumas, J.P, 2009. Study of a phase change energy storage using spherical capsules. Part II: Numerical modelling. Energy Convers. Manage., 50, 2537-2546.

Brent, A.D., Voller, V.R. , Reid, K.J., 1988. Enthalpy-Porosity Technique for Modelling Convection-Diffusion Phase Change: Application to the Melting of a Pure Metall. Numer. Heat Transfer, 13, 297–318.

Costa, M., Oliva, A., Pérez-Segarra, C.D., Alba, R., 1991. Numerical simulation of solid-liquid phase change phenomena. Comput. Meth. Appl. Mech. Eng., 91, 1123-1134.

Felix Regin , A., Solanki, S.C., Saini, J.S., 2009. An analysis of a packed bed latent heat thermal energy storage system using PCM capsules: Numerical investigation. Renewable Energy, 34, 1765-1773.

Gau C., Viskanta, R., 1986. Melting and solidification of a Pure Metal on a Vertical Wall. ASME J. Heat Transfer, 108, 174-181.

Lehmkul O., Pérez-Segarra, C.D., Borrell, R., Soria, M., Oliva, A., 2009. TermoFluids: A new Parallel unstructured CFD code for the simulation of turbulent industrial problems on low cost PC Cluster. Lect. Notes Comp. Sci., 67, 275-282.

Tan, F.L., 2008. Constrained and unconstrained melting inside a sphere. Int. Commun. Heat Mass, 35, 466-475.

Tan, F.L., Hosseinizadeh, S.F., Khodadadi, J.M., Fan, L., 2009. Experimental and computational study of constrained melting of phase change materials (PCM) inside a spherical capsule. Int. J. Heat Mass Transfer, 52, 3464–3472.

Vafai , K., Sozen, M., 1990. Analysis of energy and momentum transport for fluid flow through a porous bed. ASME J. Heat Transfer, 112, 690-699.

Vidal, B., 2007. Modelización del cambio de fase sólido líquido. Aplicación a sistemas de acumulación de energía térmica. Doctoral thesis.

Voller, V., Prakash, C., 1987. A Fixed Grid Numerical Modelling Methodology for Convection-Diffusion Mushy Region Phase Change Problems. Int. J. Heat Mass Transfer, 30, 1709–1719.

Wakao, N., Kaguei, S., Funazkri, T., 1979. Effect of fluid dispersion coefficients on particle-to-fluid heat transfer coefficients in packed beds. Chem. Eng. Sci., 34, 325-336.

Wolf, F., Viskanta, R., 1987. Melting of a pure metal froma vertical wall. Exp. Heat Transfer, 1, 17-30.

7. Acknowledgments

P.A. Galione wishes to thank the Agencia Nacional de Investigación e Innovación (ANII), Uruguay, for its financial support in the form of a master's degree scolarship.

This work has been partially funded by "Ministerio de Ciencia, Innovación y Tecnología", Spain, through the project ENE2010 – 17801.